Kirigami Mechanics as Stress Relief by Elastic Charges

Michael Moshe,[1,2,*] Edward Esposito,[3] Suraj Shankar,[2,4,†] Baris Bircan,[5] Itai Cohen,[3,‡]
David R. Nelson,[1,§] and Mark J. Bowick[2,4,∥]
[1]*Department of Physics, Harvard University, Cambridge, Massachusetts 02138, USA*
[2]*Physics Department and Syracuse Soft and Living Matter Program, Syracuse University, Syracuse, New York 13244, USA*
[3]*Laboratory of Atomic and Solid State Physics, Cornell University, Ithaca, New York 14853, USA*
[4]*Kavli Institute for Theoretical Physics, University of California, Santa Barbara, California 93106, USA*
[5]*School of Applied and Engineering Physics, Cornell University, Ithaca, New York 14853, USA*

(Received 13 August 2018; published 28 January 2019)

We develop a geometric approach to understand the mechanics of perforated thin elastic sheets, using the method of strain-dependent image elastic charges. This technique recognizes the buckling response of a hole under an external load as a geometrically tuned mechanism of stress relief. We use a diagonally pulled square paper frame as a model system to quantitatively test and validate our approach. Specifically, we compare nonlinear force-extension curves and global displacement fields in theory and experiment. We find a strong softening of the force response accompanied by curvature localization at the inner corners of the buckled frame. Counterintuitively, though in complete agreement with our theory, for a range of intermediate hole sizes, wider frames are found to buckle more easily than narrower ones. Upon extending these ideas to many holes, we demonstrate that interacting elastic image charges can provide a useful *kirigami* design principle to selectively relax stresses in elastic materials.

DOI: 10.1103/PhysRevLett.122.048001

Kirigami, the art of cutting and folding paper, has emerged as a powerful tool to dramatically modify, reconfigure, and program material properties [1–11]. Since kirigami is scale invariant, it can be combined with rapid miniaturization to design metamaterial response and structures at the smallest scales [12,13]. Such approaches were recently demonstrated in graphene [14] and now provide unprecedented opportunities for designing devices with novel electronic and mechanical properties. With the advent of such technologies, it has become increasingly important to characterize and understand the various ways material deformations accommodate and relax stress through instabilities in thin two-dimensional (2D) elastic sheets [9,15–20].

The mechanics of thin elastic sheets is controlled by the dimensionless Föppl–von Kármán (FvK) number $\gamma = YR^2/\kappa$ [21] that indicates the relative ease of in-plane stretching vs out-of-plane bending. Here R is a characteristic linear dimension of the sheet, Y the 2D Young's modulus, and κ the bending rigidity. Under an external load, a thin sheet trades energetically expensive stretching with bending to relieve stresses by either buckling [21] or wrinkling [22–24], possibly followed by secondary instabilities [17,25,26]. By introducing holes or cuts, kirigami now provides a distinct route to locally relieve stresses through these geometric features, though a general characterization of its effective mechanical response is not known. The *inverse problem* of predicting the correct kirigami pattern to relax a given prestress in a material also remains an open problem, complicated by the notorious nonlinearity inherent in thin sheet elasticity.

In this letter, we develop a geometric framework to address some of the general mechanical consequences of kirigami and report on experimental measurements of force-extension curves of pulled paper frames. A more detailed theoretical and numerical analysis is presented in a longer companion letter [27]. Starting with a single square frame, we use the technique of strain-dependent image elastic charges to show that a hole under an external load acts as a geometrically tunable source of local stress, which is relaxed by local buckling. The lowest-order image elastic charge induced in a hole is a quadrupolar singularity in Gaussian curvature [29,30]. When permitted by the shape of the hole, this singularity can fractionalize into partial disclinations, naturally explaining the curvature localization at interior corners seen experimentally for square frames. Thus, the buckling response of the sheet can be viewed as the sheet screening the image charges by adopting a curved 3D configuration that leads to a softer force response. We find consistent agreement between theory and experiment in the geometric dependence of effective spring constants (summarized in Table I) and the buckling threshold, along with local measures of deformation.

A similar buckling-induced softened mechanical response has been previously investigated in periodic arrays of slits under uniaxial tension [7,10,31]. Motivated by Ref. [9], we go beyond slits and use square holes as a

TABLE I. A summary of the effective spring constants k_{eff} for different frame aspect ratios w/L, for planar and buckled configurations.

Configuration	Aspect ratio	k_{eff}
Planar	$0 < (w/L) < 1/2$	$\propto Y[\Phi(w/L)]^2(w/L)^2$
Buckled	$\frac{1}{8} < (w/L) < \frac{1}{4}$	$\propto(\kappa/L^2)[\Phi(w/L)]^2 \ln(w/a)$
	$(w/L) < \frac{1}{8}$	$\propto(\kappa/L^2)(w/L)$

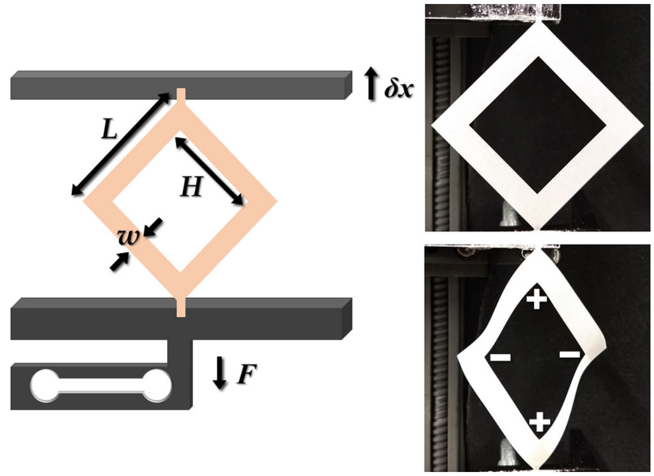

FIG. 1. Force displacement measurement. (a) Square paper frames with thin tabs on two opposite corners are glued to two opposed aluminum plates. The top plate can be displaced upward using a micrometer screw gauge for very fine displacements or using a stepper motor for larger displacements. A load cell attached to the bottom plate measures the force required to hold the frame at a fixed displacement. In our experiments, all frames had the same side length L of 5.04 cm, while the frame width $w = (L - H)/2$ was varied. (b) Planar paper frame. (c) Buckled paper frame, with labeled disclinations.

nontrivial yet simple illustration of our framework. This rationalizes previous results, extends to arbitrary hole shapes [32], and provides a systematic approach to handle many holes. In addition, collective effects arising from interactions between holes are neglected in works that just analyze the unit cell of a periodic lattice but are easily captured using the elastic charge framework. Using a flattened cone as an example, we demonstrate how interactions between image charges can guide the design of appropriate kirigami patterns to relax the preexisting stress in the system.

The square frames we study were cut from sheets of Glama Natural paper of various thicknesses ($t = 0.01$–0.02 mm) with an edge length $L = 5.04$ cm. The aspect ratio w/L, where $w = (L - H)/2$ is the frame width and H is the hole size (see Fig. 1), was varied between $0 < w/L < 1/4$ for reasons explained later. Frames with larger aspect ratios corresponding to smaller holes often tore before buckling. To measure force-extension curves, we mount the opposite outer corners of the frames between a top and bottom plate and extend them by a distance δx (Fig. 1). To generate displacements, we use a rail-guided Haydon-Kerk stepper motor to move a micrometer translation stage to which one corner of the frame is attached. Coarse displacements (~500 μm) are generated with the stepper motor, while finer displacements (~50 μm), primarily near buckling, are generated using the micrometer stage. Force measurements were made using a Loadstar parallel cantilever load cell attached to the bottom plate. Further details of the experimental protocol are given in Ref. [28]. We observe a steep increase in force at low displacements, followed by a leveling off beyond a critical displacement, and finally an increase at high displacements just before the frames tear [Fig. 2(a)].

The initial buckling can be understood within the framework of a stretching to bending transition. The mechanics of the frame is governed by an elastic energy involving both stretching and bending terms quadratic in the stress tensor ($\boldsymbol{\sigma}$) and the curvature tensor ($\mathbf{b}$). Upon minimizing, we obtain the covariant FvK equations [33,34],

$$\frac{1}{Y}\Delta\Delta\chi = K_{\text{Im}} - K_G, \tag{1a}$$

$$\kappa\Delta\text{tr}(\mathbf{b}) = \sigma^{\mu\nu}b_{\mu\nu}. \tag{1b}$$

Here we have used the 2D Airy stress function χ ($\sigma^{\alpha\beta} = \epsilon^{\alpha\mu}\epsilon^{\beta\nu}\nabla_\mu\nabla_\nu\chi$). The extrinsic curvature tensor is defined by $b_{\alpha\beta} = \hat{\mathbf{n}} \cdot \nabla_\alpha \mathbf{t}_\beta$, where $\hat{\mathbf{n}}$ and $\mathbf{t}_\beta$ are the local normal and tangent vectors to the surface, respectively, and whose determinant gives the Gaussian curvature K_G of the surface. In terms of a 3D Young's modulus $\bar{Y}$, we have $Y = \bar{Y}t$ and $\kappa = \bar{Y}t^3/[12(1-\nu^2)]$, where t is the sheet thickness and ν is the three-dimensional Poisson ratio [35]. Unlike the conventional FvK equations for thin plates, we have additionally included a source of Gaussian curvature K_{Im} that plays the same role that defects play in crystals [36], though in our case this function describes a distribution of *image* elastic charges that are induced within the hole and depend on the external load, serving to enforce the appropriate boundary conditions required by the hole [27]. Here the analogy with electrostatics helps, in that the hole under external stress functions like a conductive shell in an external electric field. This framework allows for understanding the various scalings observed in the data.

For very small diagonal displacements ($\delta x < \delta x_c$, with δx_c the buckling threshold), it is clear that the frame responds linearly by stretching [Fig. 2(b)]. Though the frame is still planar, the effective spring constant is modified by the hole geometry. Setting $\mathbf{b} = \mathbf{0}$ ($K_G = 0$), we have only K_{Im}, the image elastic charge, present within the hole. Unlike genuine topological disclinations or dislocations (monopole and dipole singularities) that *cannot* be created by any local deformation [29], the leading-order

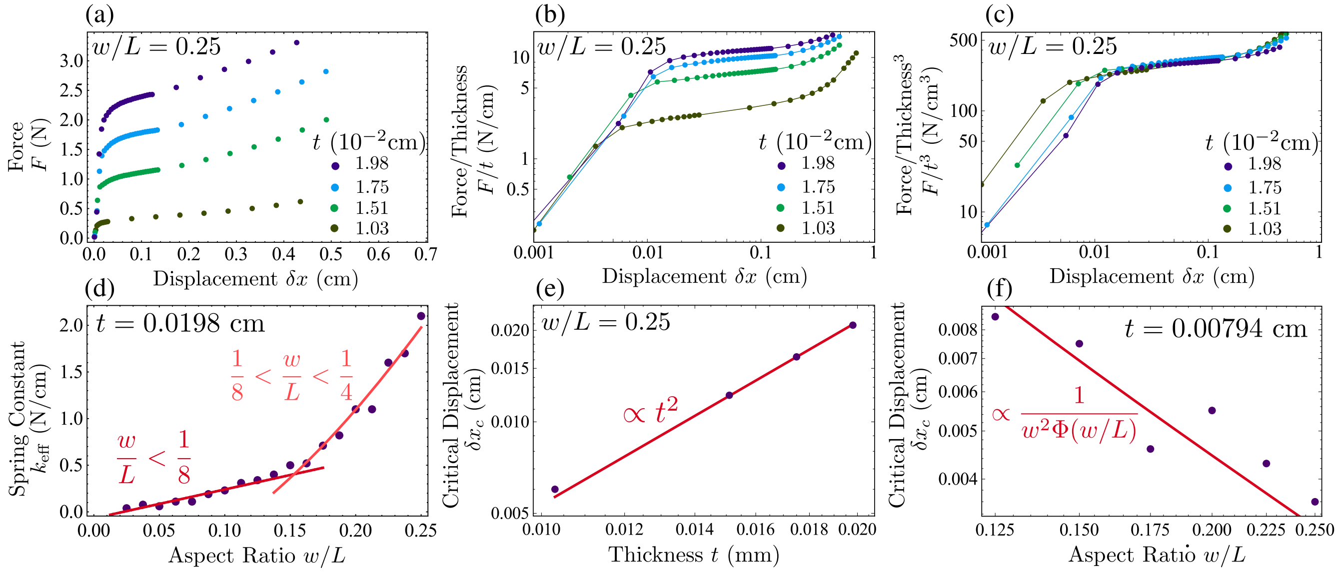

FIG. 2. Experimental measurements of square frames subjected to a tensile load along the diagonal. (a) Force-displacement curves for frames with $w/L = 0.25$ and thicknesses varying between 0.01 and 0.02 cm. (b) When normalized by thickness, curves collapse at a small displacement, confirming that the frames are planar at this regime. (c) When normalized by thickness cubed, curves collapse in the postbuckling regime, confirming that the energy increase is predominately bending. (d) Effective spring constant in the postbuckled regime as a function of frame aspect ratio w/L in the intermediate and large hole regimes for a frame of thickness $t = 0.0198$ cm, confirming the multiscale behavior in Table I. The curve in the large hole regime is linear (3), while the curve in the intermediate hole regime corresponds to (2), with the prefactor c and regularizing cutoff a taken as fitting parameters. (e) Critical displacement as a function of the thickness for a frame of $w/L = 0.25$, growing as $t^{1.9}$ (solid line), in good agreement with Eq. (4). (f) Critical displacement as a function of the frame's aspect ratio for a frame of thickness $t = 0.00794$ cm in the intermediate hole size regime, in agreement with Eq. (4) (solid line).

contribution to K_{Im} is of quadrupolar form [30]. In 2D the quadrupole is written as $Q_{ij} = Q(2\hat{d}_i\hat{d}_j - \delta_{ij})$ with $\hat{\mathbf{d}} = (\cos\psi, \sin\psi)$, ψ being its orientation and Q its magnitude. In the presence of sharp corners in the hole geometry, the induced image elastic charge can fractionalize into *partial* disclinations that localize at the corners, just as in the electrostatic analogue, and generate stress fields similar to their topological counterparts [37]. The partial disclinations have a charge that continuously depends on the external strain imposed, given by $s \equiv Q/H^2 = (\delta x/L)\Phi(w/L)$, where $\Phi(w/L)$ is a rational function of the frame's aspect ratio that encodes the hole geometry [27]. As $w \to L/2$ (no hole), $\Phi(w/L) \propto (1 - 2w/L)^2$ vanishes as expected and remains finite in the opposite narrow frame limit ($w \to 0$). This setup allows us to estimate the energy due to stretching and bending.

Prior to buckling, the elastic energy of the planar square frame is approximately $E \sim Ys^2w^2$. For large displacements, the frame buckles, allowing $K_G \neq 0$. As the frame's large FvK number ($\gamma = Yw^2/\kappa \gg 1$) favors isometric deformations, the frame screens out the induced image charge K_{Im} with real Gaussian curvature K_G [37], permitting the stress-free state $\chi = 0$ to become available. By virtue of the localized partial disclinations, the buckled frame adopts a locally conical shape near the inner corners leading to the energy being $E \sim \kappa[c_1 s + c_2 s^2]\ln(w/a)$, where $a \sim t$ is a microscopic core cutoff and c_1 and c_2 are numerical constants [37]. Since $F = dE/d\delta x$, we rescale the force-extension curve by t and t^3 for a given aspect ratio ($w/L = 0.25$) in Figs. 2(b) and 2(c). We find excellent collapse in the prebuckling and postbuckling regimes, which are controlled by Y and κ, respectively. The t^3 scaling in the postbuckling plateau indicates the force response is governed by κ and the hole geometry alone.

The fractionalized quadrupole naturally delineates different geometric regimes. For $w/L < 1/4$, the partial disclinations remain well separated and essentially noninteracting, allowing one to approximately superpose their buckled solutions, while for narrower frames with $w/L < 1/8$ [27], higher-order charges become important. Within the intermediate frame regime ($1/8 < w/L < 1/4$), the effective linearized spring constant of the frame postbuckling is then given as

$$k_{\text{eff}} = \left.\frac{d^2E}{d\delta x^2}\right|_0 \propto \frac{\kappa}{L^2}\ln\left(\frac{w}{a}\right)[\Phi(w/L)]^2. \tag{2}$$

To calculate the buckled force response of narrow frames ($w/L < 1/8$), we use an alternate approach. Here, an infinite series of multipolar charges higher than the quadrupole become important, suggesting that the appropriate weakly interacting degrees of freedom are not elastic charges. Instead, we treat the frame edges as quasi-1D ribbons joined in a ring. Neglecting the high-energy splay modes, the bending and twisting elastic energy of a ribbon is approximated by $E \sim \kappa w L(\delta\theta/L)^2$, where $\delta\theta \propto \delta x/L$ is the net rotation of the ribbon across its length [35]. Once again computing the effective linearized spring constant for the buckled narrow frames, we obtain

$$k_{\text{eff}} \propto \frac{\kappa w}{L^3}. \tag{3}$$

The disparate geometry-controlled scaling of k_{eff} for different frame widths [Eqs. (2) and (3)] is a signature of multiscale behavior. We fit the experimentally measured spring constants of the buckled frames to the theoretical expressions for k_{eff} as shown in Fig. 2(d), with good agreement. The geometric dependence of various linearized spring constants is also summarized for both buckled and planar frames in Table I.

For intermediate frame widths $1/8 < w/L < 1/4$, given that the frame mechanics is dictated by the partial disclinations, we can estimate the geometry dependence of the frame's buckling threshold δx_c by adapting previous results on the buckling of topological disclinations [37]. As the region of influence of the partial disclination is a corner plaquette of area $\sim w^2$, using the relevant FvK number $\gamma = Yw^2/\kappa$, we obtain a threshold charge $|s_c| \simeq \gamma_c/\gamma$ in order to buckle ($\gamma_c \approx 120$ for topological disclinations; also see [27]). Upon using $s = (\delta x/L)\Phi(w/L)$, we find the critical strain:

$$\frac{\delta x_c}{L} \propto \frac{1}{\Phi(w/L)}\left(\frac{t}{w}\right)^2, \tag{4}$$

where we have used the fact that $\kappa/Y \propto t^2$. The quadratic scaling of δx_c with t is consistent with observed data [Fig. 2(e)], with δx_c determined by the intersection of linear fits to the data just before and after the transition. The dependence of δx_c on the frame width w crucially captures the geometric tunability of the local propensity to relax stresses via buckling. Though we expect ultranarrow frames ($w \to 0$) to have a vanishing threshold for buckling [38] due to sheer loss of material, within the intermediate range of hole sizes Eq. (4), in fact, suggests a counterintuitive trend, with wider frames buckling prior to narrow ones. This feature is observed for a thin enough sheet in Fig. 2(f).

Apart from the above global characterizations of frame mechanics, we also probe local measures such as the nonuniform displacement field over the entire frame, thereby allowing for a stronger test of the theory. Using grid lines etched into the paper, painted black to improve the contrast in imaging, we measure the displacement field of the frame by comparing its projected mesh just past buckling to a reference undeformed mesh. As the uniaxial tensile load prescribes the orientation of the induced quadrupoles, with just the scalar charge magnitudes as fitting parameters [39], we find that the entire spatial deformation field is well captured within our image charge framework (red lines in Fig. 3) [27].

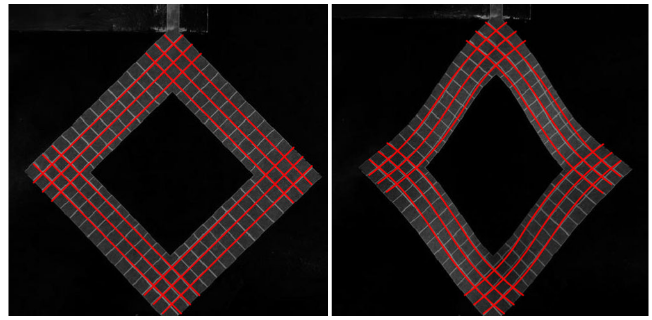

FIG. 3. Comparison between predicted and observed deformations in a buckled frame. (a) An undeformed frame with laser-printed Cartesian mesh (gray) and a set of parametric lines (red) fitted to the printed mesh. (b) A deformed frame. Here, the red lines are computed from the theory using the original parametric lines as a starting point and fictitious elastic charges as fitting parameters.

The quantitative success of our theory in describing the mechanics of isolated frames encourages us to take a step further and exploit the method of charges to analyze kirigami patterns, which now involves interactions between the charges in different holes. The elastic interaction energy of two planar quadrupoles $\mathbf{Q}_1$ and $\mathbf{Q}_2$ a distance $\mathbf{r}$ apart is given by [40,41]

$$E_{\text{int}} = \frac{YQ_1Q_2}{\pi r^2}\cos(2\psi_1 + 2\psi_2), \tag{5}$$

where the quadrupole angles ψ_1 and ψ_2 are with respect to the pair separation $\mathbf{r}$. To demonstrate that interacting elastic charges can fruitfully guide design of kirigami metamaterials, we shall focus on the simple problem of a flattened cone as an example of the inverse problem in kirigami mechanics. A conical frustum (with either an angle deficit or excess) when confined with a small gap in the plane is stressed due to its intrinsic geometry, a state that can be relaxed for a sufficiently thin sheet by wrinkling [Fig. 4(a)]. Patterning an appropriate kirigami design affords the sheet a new mechanism of locally relaxing in-plane stress *without* wrinkling. For the regular circular cone, minimizing the energy of an interacting pair of quadrupoles with the background stress field of a positive disclination, we find (see [28]) that the equilibrium configuration favors azimuthally aligned quadrupoles. Unlike squares that lock the quadrupole orientation to their diagonals, slits permit quadrupolar charges only perpendicular to their long axis. Hence, while azimuthal slits leave the wrinkles unaltered [Fig. 4(b)], radial slits in a staggered array (which minimizes the charge-charge interactions) around the cone

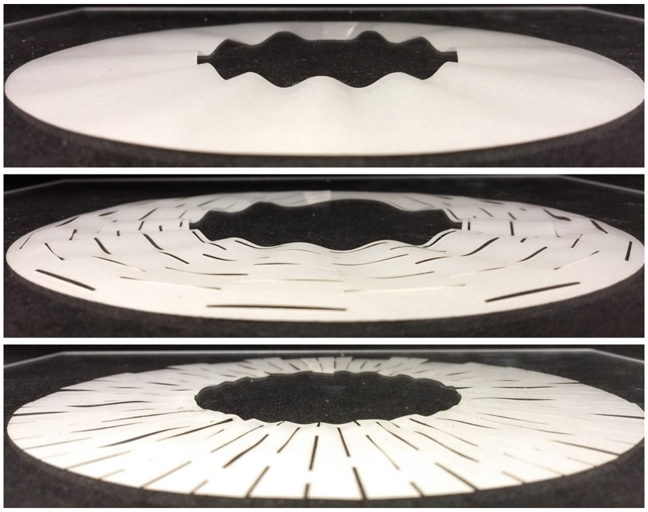

FIG. 4. (a) A conical annulus flattened under a piece of acrylic, with a small gap allowing for wrinkle formation. (b) Azimuthal slits do not affect the pattern of wrinkles. (c) Radial slits result in azimuthal quadrupoles, minimizing interaction energy with the curvature monopole. When flattened, radial slits lead to a soft response with no wrinkles.

locally relax stress when flattened [Fig. 4(c)]. Similar slit patterns also relax stresses in a flattened *e*-cone [42] as shown in [28].

In summary, we have proposed a useful elastic charge framework to understand kirigami mechanics in thin sheets with perforations. By relating the challenging nonlinear problem of postbuckling mechanics to the simpler prebuckling computation within the planar problem, we are able to quantitatively test the analytical predictions against experimental measurements through both global and local measures of deformation. The inclusion of interactions between charges also suggests that our framework can advise possible design strategies to pattern kirigami metamaterials that permit engineering pathways to locally relax elastic stresses. Addressing nonlinear and thermal effects are promising directions for future work.

We thank James Pikul, Marc Miskin, and Winston Lee, for their valuable insights and help with guiding the initial experiments. We thank Paul McEuen, Kyle Dorsey, Tanner Pearson, and Zeb Rocklin for very useful conversations throughout the project. Work by I. C. was supported by a grant from the NSF DMREF program under Grant No. DMR-1435829. Work by M. J. B. was supported by the KITP Grant No. PHY-1125915, KITP NSF Grant No. PHY-1748958, and the NSF DMREF program, via Grant No. DMREF-1435794. Work by D. R. N. was primarily supported through the NSF DMREF program, via Grant No. DMREF-1435999, as well as in part through the Harvard Materials Research and Engineering Center, via NSF Grant No. DMR-1420570. M. M. acknowledges the USIEF Fulbright program. M. M., S. S., and M. J. B. thank the Syracuse Soft & Living Matter Program for support and the KITP for hospitality during completion of some of this work.

[*]michael.moshe@mail.huji.ac.il
Present address: Racah Institute of Physics, Hebrew University of Jerusalem, Jerusalem 91904, Israel
[†]sushanka@syr.edu
[‡]itai.cohen@cornell.edu
[§]nelson@physics.harvard.edu
[‖]bowick@kitp.ucsb.edu

[1] T. Mullin, S. Deschanel, K. Bertoldi, and M. C. Boyce, Phys. Rev. Lett. **99**, 084301 (2007).
[2] K. Bertoldi, P. M. Reis, S. Willshaw, and T. Mullin, Adv. Mater. **22**, 361 (2010).
[3] B. Florijn, C. Coulais, and M. van Hecke, Phys. Rev. Lett. **113**, 175503 (2014).
[4] Z. Song, X. Wang, C. Lv, Y. An, M. Liang, T. Ma, D. He, Y.-J. Zheng, S.-Q. Huang, H. Yu *et al.*, Sci. Rep. **5**, 10988 (2015).
[5] Y. Zhang, Z. Yan, K. Nan, D. Xiao, Y. Liu, H. Luan, H. Fu, X. Wang, Q. Yang, J. Wang *et al.*, Proc. Natl. Acad. Sci. U.S.A. **112**, 11757 (2015).
[6] A. Lamoureux, K. Lee, M. Shlian, S. R. Forrest, and M. Shtein, Nat. Commun. **6**, 8092 (2015).
[7] T. C. Shyu, P. F. Damasceno, P. M. Dodd, A. Lamoureux, L. Xu, M. Shlian, M. Shtein, S. C. Glotzer, and N. A. Kotov, Nat. Mater. **14**, 785 (2015).
[8] C. Wu, X. Wang, L. Lin, H. Guo, and Z. L. Wang, ACS Nano **10**, 4652 (2016).
[9] M. A. Dias, M. P. McCarron, D. Rayneau-Kirkhope, P. Z. Hanakata, D. K. Campbell, H. S. Park, and D. P. Holmes, Soft Matter **13**, 9087 (2017).
[10] A. Rafsanjani and K. Bertoldi, Phys. Rev. Lett. **118**, 084301 (2017).
[11] P. Z. Hanakata, Z. Qi, D. K. Campbell, and H. S. Park, Nanoscale **8**, 458 (2016).
[12] J. A. Rogers and Y. Huang, Proc. Natl. Acad. Sci. U.S.A. **106**, 10875 (2009).
[13] S. Deng and V. Berry, Mater. Today **19**, 197 (2016).
[14] M. K. Blees, A. W. Barnard, P. A. Rose, S. P. Roberts, K. L. McGill, P. Y. Huang, A. R. Ruyack, J. W. Kevek, B. Kobrin, D. A. Muller *et al.*, Nature (London) **524**, 204 (2015).
[15] E. Sharon, M. Marder, and H. L. Swinney, Am. Sci. **92**, 254 (2004).
[16] J. Genzer and J. Groenewold, Soft Matter **2**, 310 (2006).
[17] T. A. Witten, Rev. Mod. Phys. **79**, 643 (2007).
[18] B. Li, Y.-P. Cao, X.-Q. Feng, and H. Gao, Soft Matter **8**, 5728 (2012).
[19] P. M. Reis, H. M. Jaeger, and M. van Hecke, Extreme Mech. Lett. **5**, 25 (2015).
[20] K. Bertoldi, V. Vitelli, J. Christensen, and M. van Hecke, Nat. Rev. Mater. **2**, 17066 (2017).
[21] L. D. Landau and E. Lifshitz, *Theory of Elasticity* (Elsevier, New York, 1986), Vol. 3.
[22] E. Cerda, K. Ravi-Chandar, and L. Mahadevan, Nature (London) **419**, 579 (2002).
[23] E. Cerda and L. Mahadevan, Phys. Rev. Lett. **90**, 074302 (2003).

[24] H. King, R. D. Schroll, B. Davidovitch, and N. Menon, Proc. Natl. Acad. Sci. U.S.A. **109**, 9716 (2012).

[25] M. Ben Amar and Y. Pomeau, Proc. R. Soc. A **453**, 729 (1997).

[26] L. Pocivavsek, R. Dellsy, A. Kern, S. Johnson, B. Lin, K. Y. C. Lee, and E. Cerda, Science **320**, 912 (2008).

[27] M. Moshe, E. Esposito, S. Shankar, B. Bircan, I. Cohen, D. R. Nelson, and M. J. Bowick, Phys. Rev. E **99**, 013002 (2019); also see *Mathematica* notebook in Supplemental Material for detailed computations.

[28] See Supplemental Material at http://link.aps.org/supplemental/10.1103/PhysRevLett.122.048001 for more details about experimental protocol and theory of interacting quadrupoles.

[29] R. Kupferman, M. Moshe, and J. P. Solomon, ARMA **216**, 1009 (2013).

[30] M. Moshe, I. Levin, H. Aharoni, R. Kupferman, and E. Sharon, Proc. Natl. Acad. Sci. U.S.A. **112**, 10873 (2015).

[31] M. Isobe and K. Okumura, Sci. Rep. **6**, 24758 (2016).

[32] Our focus is mainly on square holes, because the concentration of elastic charges at sharp corners simplifies the analysis; elastic charges are delocalized around the rim when one considers, say, circular holes instead [27].

[33] W. T. Koiter, Proc. Koninkl. Ned. Akad. van Wetenschappen, Series B **69**, 1 (1966); See also A. M. A. van der Heijden, *W. T. Koiter's Elastic Stability of Solids and Structures* (Cambridge University Press, Cambridge, England, 2009).

[34] P. G. Ciarlet, *Mathematical Elasticity: Theory of Plates* (North-Holland, Amsterdam, 1997).

[35] B. Audoly and Y. Pomeau, *Elasticity and Geometry: From Hair Curls to the Non-Linear Response of Shells* (Oxford University Press, Oxford, United Kingdom, 2010).

[36] D. R. Nelson, *Defects and Geometry in Condensed Matter Physics* (Cambridge University Press, Cambridge, England, 2002).

[37] H. S. Seung and D. R. Nelson, Phys. Rev. A **38**, 1005 (1988).

[38] Buckling of narrow frames modeled as coupled ribbons is not obtained by balancing global estimates of bending and stretching energy, both being quadratic in δx. Instead, nonlinearity and local buckling are important.

[39] Close to the threshold, charges are only partially screened, hence the fit. Note the deformation is nonetheless still described by a quadrupole.

[40] E. A. Matsumoto and R. D. Kamien, Phys. Rev. E **80**, 021604 (2009).

[41] M. Moshe, E. Sharon, and R. Kupferman, Phys. Rev. E **92**, 062403 (2015).

[42] M. M. Müller, M. B. Amar, and J. Guven, Phys. Rev. Lett. **101**, 156104 (2008).